Intensity Variations in Potential Vorticity Streamers:

Development Pathways and Environmental Impacts in the North Atlantic Basin

18th Cyclone Workshop
Hotel Mont Gabriel, Sainte Adele,
Quebec, Canada: 1–6 October 2017

Philippe P. Papin*, Lance F. Bosart, Ryan D. Torn

Department of Atmospheric and Environmental Sciences
University at Albany, SUNY, Albany, NY

*Corresponding author email:
ppapin@albany.edu

1) Introduction

- Potential vorticity streamers (PVSs) in the upper-troposphere are positively-tilted troughs that form in response to anticyclonic Rossby wave breaking (RWB) in the Atlantic basin (Fig. 1)
- PVSs modify the local environment by:
  1. Enhancing vertical wind shear (VWS) corridors
  2. Enhancing +/- moisture anomalies
     - These factors are known to influence tropical cyclone (TC) activity in the Atlantic basin
- This study will investigate:
  1. Summertime PVS activity - combining frequency, intensity, and size
  2. Composite differences between strong and weak PVSs of similar size and orientation
  3. How active and inactive PVS years spatially modulate TC activity and tropical cyclogenesis (TCG) pathways

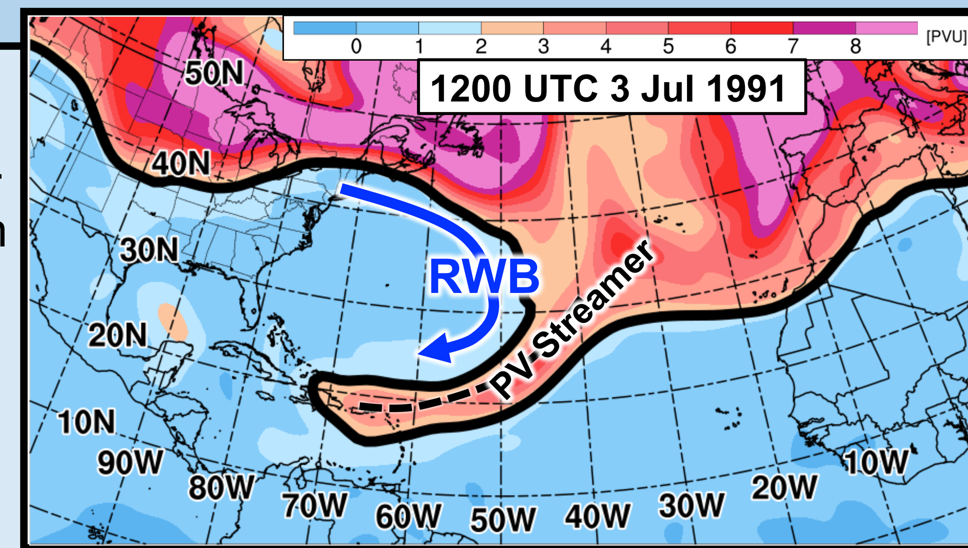

Fig. 1. An example of a PVS on 1200 UTC 3 July 1991. Plotted is 350-K PV (shaded, PVU) and the 2-PVU contour (black line). RWB is illustrated as the folding over of the 2-PVU contour (blue arrow).

2) PV Streamer Identification

Fig. 2. Schematic example of how a PVS is identified. The black line is the 2-PVU contour on the 350-K isentropic surface, with annotations provided by the key at the bottom of the figure.

- Identification technique adapted from prior methodologies in order to link PVS areas to RWB occurrence (Postal and Hitchman et al. 1999, Wernli and Sprenger 2007)
- **Dataset:** ERA-Interim coarsened to 2.5° resolution
- PVSs identified by this technique are categorized by their area, intensity, and orientation
- The intensity of each PVS identified is calculated as a standardized anomaly of all the grid points inside the PVS area:

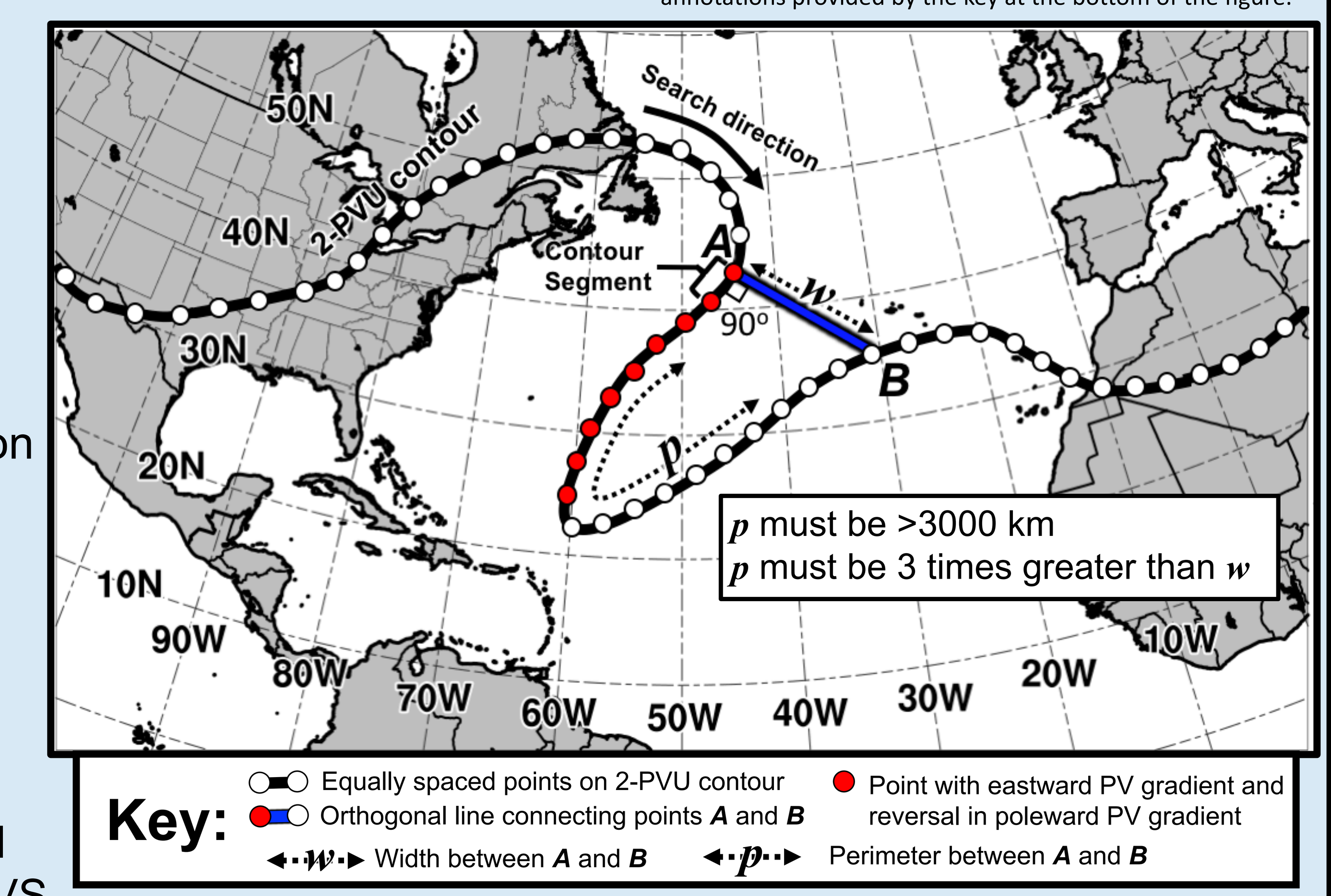

$$PV_{std\_anom} = (PV - PV_{mean\_climo}) / PV_{standard\_deviation\_climo}$$

3) Climatological Results

1979–2015, 1 Jun–30 Nov, 100-10°W

Fig. 3. Probability of PVS occurrence at every six hours from 1 June – 30 Nov (color shading, %), time-mean 200-hPa wind magnitude (yellow contours, >20 m s⁻¹) and streamlines (black arrow lines).

$$PVS\ activity\ index = \iint PV_{std\_anom}\, dA dt$$

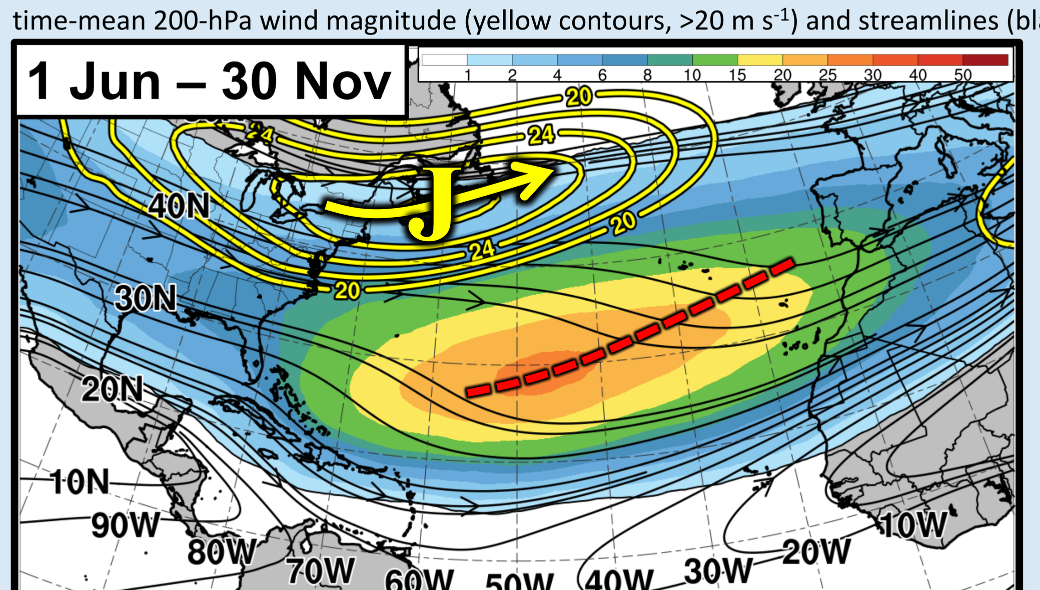

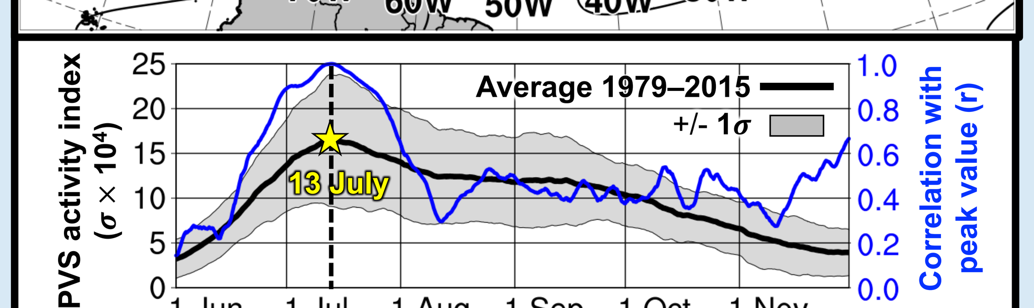

Fig. 4. 30-day running sum of PVS activity centered on each time from 1 Jun–30 Nov. Correlation with peak value (yellow star) for each date is given by the blue line.

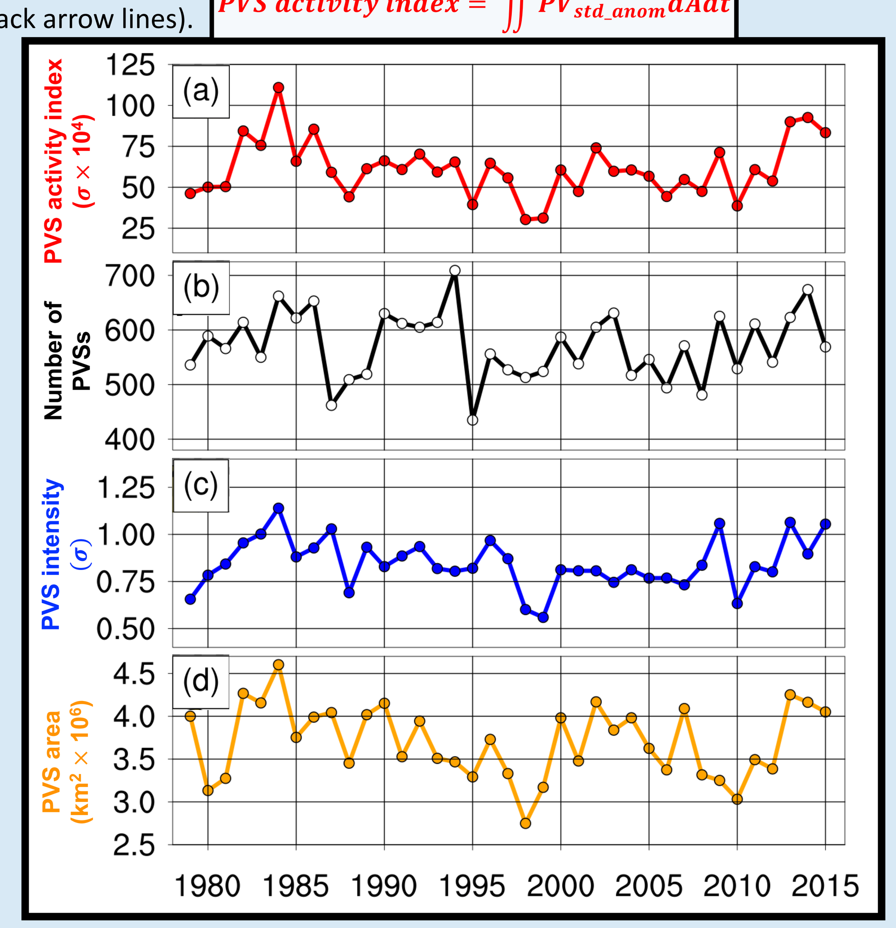

Fig. 5. 1979 – 2015 PVS time series for (a) activity index, (b) total number of PVS, (c) average intensity, and (d) average area.

4) Composite Results

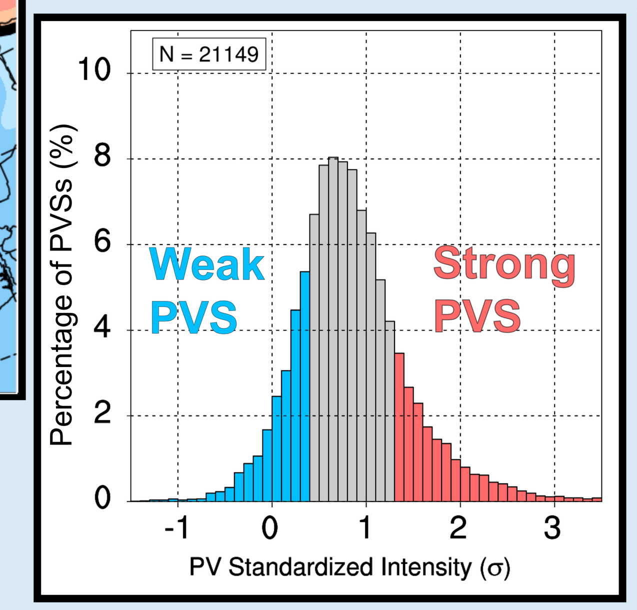

Fig. 6 Probability distribution function of PVS intensities, with top and bottom 20 percentile highlighted in red and blue respectively.

Fig. 7. Time-lagged composite evolution of strong and weak PVSs from 3 days prior (t_0 – 72h) to time of identification (t_0) in 24hr increments. Plotted are 350-K PV anomalies (shaded, PVU), 200-hPa total wind anomalies (yellow contours, > 4 m s⁻¹) and direction (vectors, m s⁻¹). Red and blue lines denote the composite 2-PVU contour for strong and weak PVSs respectively. Coordinates relative to PVS centroid at t_0 (0,0).

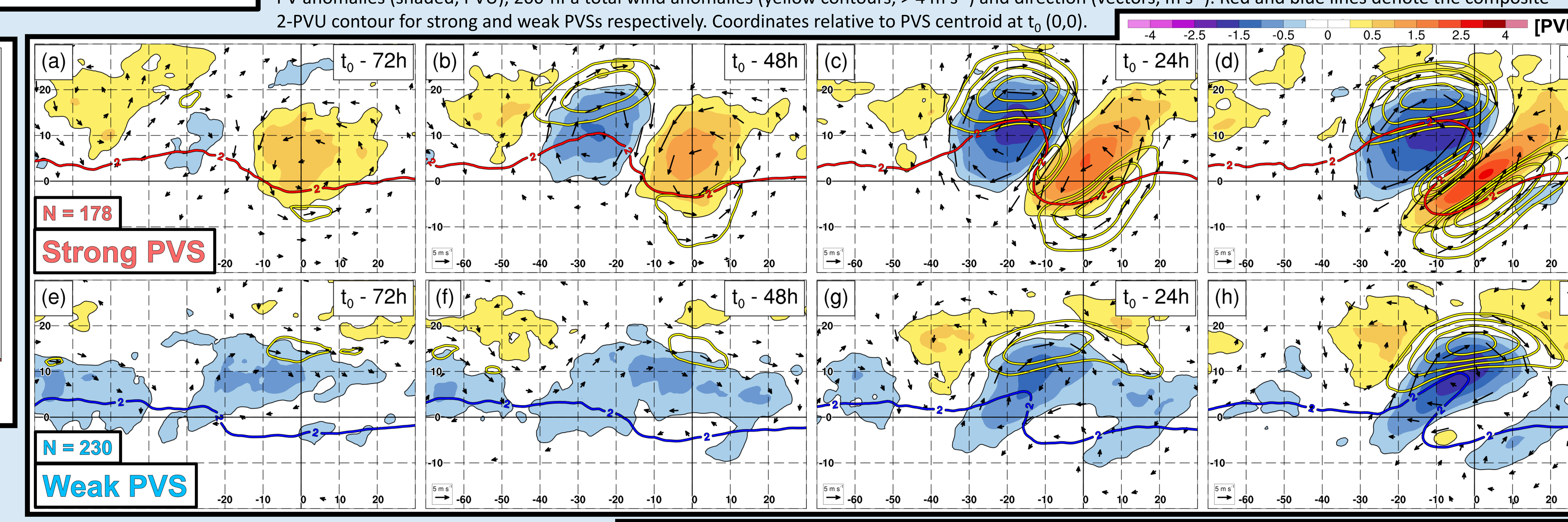

- Strong and weak PVS cases are selected from the top and bottom 20th percentiles of PVS intensity (Fig. 6)
- Only PVS cases with similar area (40-60th percentile) and orientation (40-60th percentile) are used for compositing (not shown).

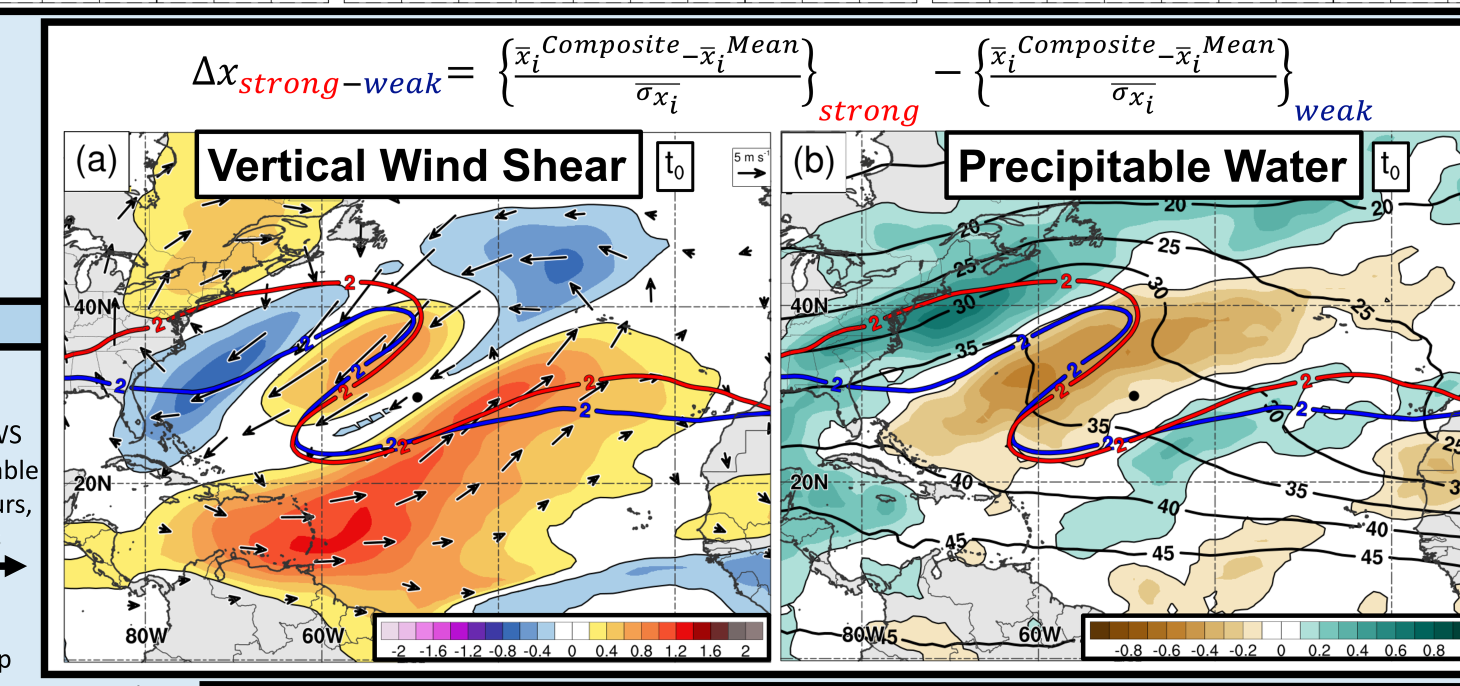

5) Impacts on TC Activity

Fig. 8. Composite standardized differences of strong minus weak PVSs at t_0 for (a) 200–850-hPa VWS anomaly (shaded, σ) and direction (vectors, m s⁻¹), (b) precipitable water anomaly (shaded, σ), and composite mean (black contours, mm). The composite 2-PVU contour of strong and weak PVSs is outlined in red and blue contours, respectively.

$$\Delta x_{strong-weak} = \left\{\frac{\bar{x}_i^{Composite} - \bar{x}_i^{Mean}}{\sigma_{\bar{x}_i}}\right\}_{strong} - \left\{\frac{\bar{x}_i^{Composite} - \bar{x}_i^{Mean}}{\sigma_{\bar{x}_i}}\right\}_{weak}$$

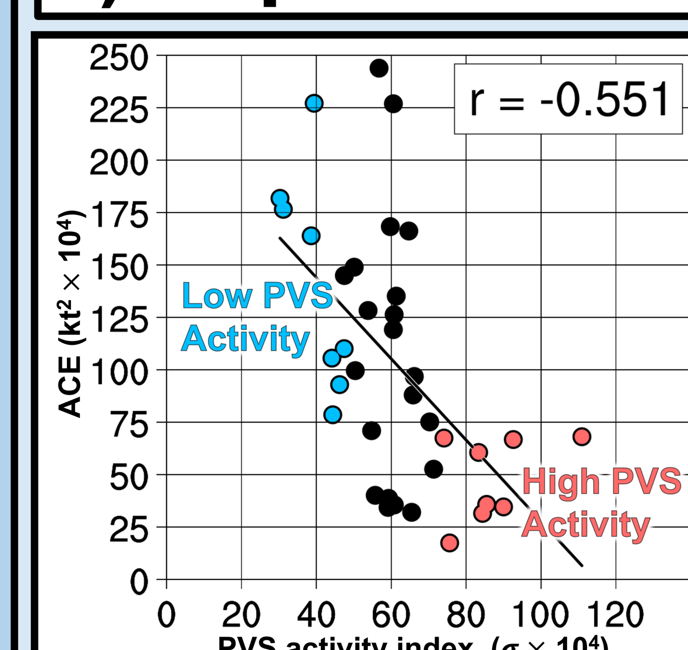

Fig. 9. Scatterplot comparing PVS activity metric (x-axis) with accumulated cyclone energy (ACE, y-axis). Correlation value (**r**) at top right with top and bottom 8 ACE seasons highlighted in red and blue, respectively.

- **Top 8** and **Bottom 8** PVS activity years selected

High PVS Activity Years:
1984,1986, 1982, 1983, 2002, 2009, 1992, 1990
Low PVS Activity Years:
1998, 1999, 2010, 1995, 1988, 2006, 1979, 2001

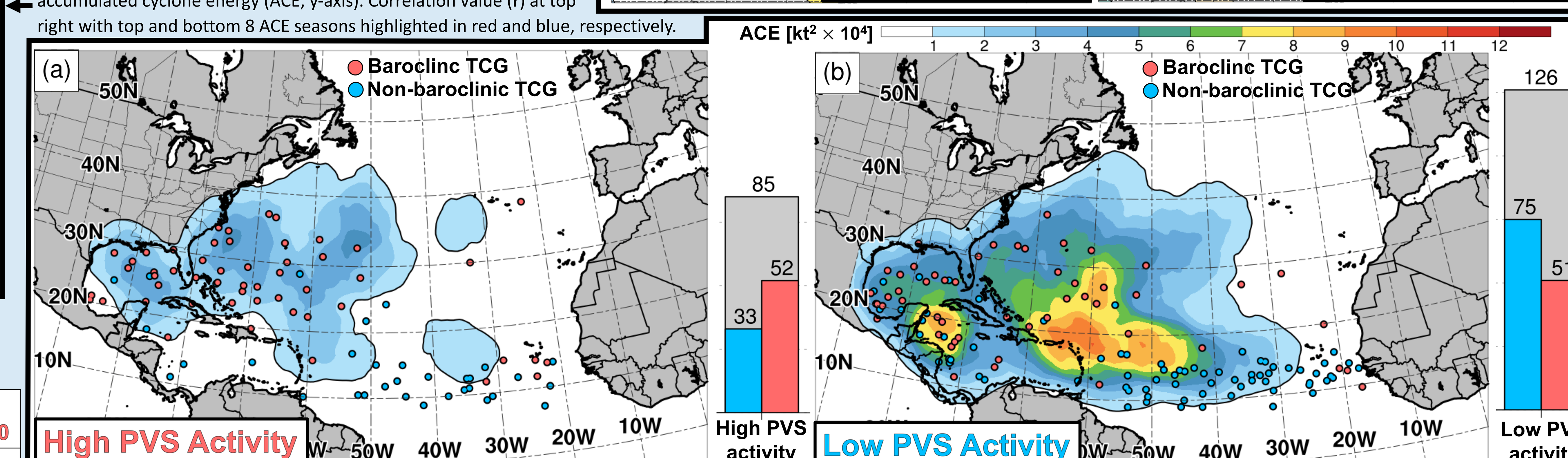

Fig. 10. Map of total seasonal ACE in a 500-km radius of each grid point (shading, kt² x10⁴) averaged for (a) high PVS activity years and (b) low PVS activity years. Circles represent genesis points of baroclinic (red) and non-baroclinic (blue) TCs. Bar plots right of map show total number of baroclinic (red), non-baroclinic (blue), and all TCG events for high and low PVS activity years.

6) Discussion and Conclusions

- Highest PVS frequency in the central Atlantic (30°N, 45°W) overlaps the midocean trough, and occurs equatorward of the 200-hPa jet (Fig. 3)
- PVS activity peaks in July, with peak activity positively correlated to PVS activity later in the season (Fig. 4)
- Large year-to-year variance in PVS activity (Fig. 5a) due to changes in frequency (Fig. 5b), intensity (Fig. 5c), and size (Fig. 5d)
- Strong PVSs develop in a +PV anomaly environment (Fig. 7a–d) while weak PVSs develop in a -PV anomaly environment (Fig. 7e–h)
- Strong PVSs have greater and more widespread southwesterly VWS anomalies downstream (Fig. 8a), and reduced precipitable water anomalies upstream of their trough axis (Fig. 8b)
- Seasonal accumulated cyclone energy (ACE) is negatively correlated with PVS activity (Fig. 9)
- TC activity is suppressed and shifted poleward in high PVS activity years due to the suppression of non-baroclinic TCG (Fig. 10a)
- TC activity is enhanced and shifted equatorward in low PVS activity years due to enhancement of non-baroclinic TCG (Fig. 10b)

Note: TCG pathways adapted from McTaggart-Cowan et al. (2013) resorted into - **Non-baroclinic events** (low-level baroclinic and non-baroclinic) **Baroclinic events** (trough-induced, weak tropical transition, and strong tropical transition)

- In conclusion, PVSs are an important feature of the summer Atlantic basin where their enhancement negatively modifies the environment to suppress non-baroclinic TC activity.

References

Funding provided by NSF Grant AGS-1656406

McTaggart-Cowan, R., T. J. Galarneau, L. F. Bosart, R. W. Moore, and O. Martius, 2013: A Global Climatology of Baroclinically Influenced Tropical Cyclogenesis. *Mon. Wea. Rev.*, **141**, 1963–1989.
Postel, G. A., and M. H. Hitchman, 1999: A Climatology of Rossby Wave Breaking along the Subtropical Tropopause. *J. Atmos. Sci.*, **56**, 359–373.
Wernli, H., and M. Sprenger, 2007: Identification and ERA-15 Climatology of Potential Vorticity Streamers and Cutoffs near the Extratropical Tropopause. *J. Atmos. Sci.*, **64**, 1569–1586.